

This is the peer reviewed version of the following article:

Concrete beams stiffened by polymer-based mortar layers: experimental investigation and modelling / Lanzoni, Luca; Soragni, Marco; Tarantino, Angelo Marcello; Viviani, M.. - In: CONSTRUCTION AND BUILDING MATERIALS. - ISSN 0950-0618. - 105:(2016), pp. 321-335. [10.1016/j.conbuildmat.2015.12.065]

Terms of use:

The terms and conditions for the reuse of this version of the manuscript are specified in the publishing policy. For all terms of use and more information see the publisher's website.

07/01/2026 11:16

Concrete beams stiffened by polymer-based mortar layers: experimental investigation and modelling

Luca Lanzoni^{a,b}, Marco Soragni^b, Angelo Marcello Tarantino^b, Marco Viviani^c

^a*DET - Dipartimento di Economia e Tecnologia, University of San Marino, Salita alla Rocca 44, Republic of San Marino, 47890 San Marino*

^b*DIEF-Department of Engineering "Enzo Ferrari", University of Modena and Reggio Emilia, 41125 Modena, Italy*

^c*HEIG-VD - Haute Ecole d'Ingénierie et de Gestion du Canton de Vaud, Route de Cheseaux 1, CH-1401 Yverdon*

Abstract

In the present work, the main results provided by an experimental investigation, assessing the mechanical performances of concrete elements stiffened by a single or more layers of different kinds of polymer-modified cementitious repair mortar, are presented. The study is aimed in order to investigate the failure mechanism occurring in the samples under bending loading. In particular, the experimental investigation allows checking if the collapse mechanism is driven by delamination occurring along the interface among the overlays or by cracks propagating from the tensile region to the compressive zone, as it occurs in a typical failure mechanism driven by flexure. Thirty-eight precast and pre-stressed concrete samples were realized and cured to simulate load-bearing concrete ceiling beams widely employed as floor systems for residential buildings. After curing, the samples were subjected to three-point loading bending tests in order to evaluate the mechanical response of the specimens in terms of load vs. mid-span transverse displacement. Through the experimental tests, the crack initiation and propagation during the bending loading have been also investigated. Simplified finite element (FE) models were performed to properly reproduce the actual response of ceiling beams under non-symmetric loading bending. It is shown that the proposed FE model can be straightforwardly used to predict the behaviour

Email address: `luca.lanzoni@unimo.it` (Luca Lanzoni)



Figure 1: Ceiling beams for flooring stiffened by a casted repairing mortar layer.

of concrete beams stiffened by polymer-based repair mortar layers.

Keywords: Repair mortar; delamination; damage process; concrete ceiling beam; non-symmetric bending test; FE models.

1. Introduction

Concrete structures and concrete structural members are prone to various kinds of degradation phenomena. Physical, chemical and biological degradation as well as excess of loads might reduce the performances and the lifespan of a concrete structure (e.g. Mehta et al. 2013 [20]). Degradations might impose to the structure owner a simple, ordinary maintenance (such as concrete patching) or, in extreme cases, the structure demolition and reconstruction. Often, a change of the utilization of a structure implies an attentive evaluation of the structural response under a new set of loads. The service load and the residual service life have to be considered carefully.

In many countries, such as Italy, reinforced concrete (RC) frames are preferred structural members to construct residential and commercial buildings. Therefore, the maintenance and reinforcement of these structural elements is a key issue. There are different kinds of reinforcement methods suitable to strengthen a concrete frame; one of the most popular is the Fibre Reinforced Polymer (FRP) retrofitting. In recent years, FRP retrofitting proved to be a reliable and efficient technique to improve both strength and load carrying capacity of concrete structural members like beams, columns, etc.

Floors of existing buildings consist of precast, pre-stressed, load-bearing concrete ceiling beams among which ceiling bricks are placed. This kind of floors can be stiffened by removing the overlying tile and applying one or

more layers of repair mortar on the upper surface of the concrete ceiling beams, as shown in (see Fig. 1). This repair process is aimed to increase the stiffness and flexural strength of the floor by casting one or more layers of repair mortar, thus preventing excessive deformation of the floor itself, failures and other damaging phenomena and, in turn, increasing the service life of the structure ¹. Before casting the repair mortar layers on the ceiling beams of a floor, the existing pavement must be removed and the intrados of the ceiling beams cleaned, making them free of cracked portions and detached parts. As expected, important issues related to the efficiency of this method of consolidation deal with the kind of the surface of the existing elements, the type of repair mortar, the presence of shear connectors, the use of bonding agents and the technique adopted to realize the strengthening (e.g. Wall 1988 [31]).

As known, the adhesive plays a crucial role in order to efficiently transfer the stresses from the strengthened element to the stiffening layer. Indeed, the success of the consolidation based on the use of repair mortar lies in the level of adhesion between the existing element and the reinforcing layer of repair mortar. Owing to this fact, the intrados of the beam should be provided with a micro or macro-texture to improve adhesion and bonding of the repairing cast to the existing elements and, in turn, the efficiency of the gluing (Júlio et al., 2004 [13]; Courard et al., 2014 [8]). Metallic anchors and shear connectors can be used to this aim too. These expedients are necessary due to the high shear stresses arising at the interface among the layers, as revealed by the analysis of the contact problem among coatings, beams and plates bonded to an elastic substrate (e.g. Lanzoni (2011) [14], Nobili and Lanzoni (2014) [22]). Since a good level of adhesion is generally difficult to accomplish (Courard et al., 2010 [7]), in the last years various kind of bonding agents (with particular reference to agents based on synthetic primers) have been studied in order to avoid delamination and crack formation at the interface. Several experimental studies can be found in literature aimed to evaluate the resistance as well as the crack formation and propagation in layered elements under bending, with specific reference to mode I, mode II and mixed-mode I/II crack formation and growth at the interface (e.g. Geissert et al., 1999 [11]; Rikards et al., 1996 [24]). Furthermore, a wide

¹Concerning the mechanical theory of damaged bodies see, for example, Lanzoni and Tarantino, 2014a-b [16], [17]

range of experimental methods exist in order to evaluate the bond strength between a substrate and an overlay (e.g. Geissert et al., 1999 [11]; Austin et al., 1995 [2]; Momayez et al. 2004 [19], Tayeh et al., 2013 [26]; Qian et al., 2014 [23]). However, as shown by Momayez et al. (2005) [18], significant differences in the adhesion evaluation can occur depending on the experimental method adopted to assess the bond strength. In particular, these Authors investigated the effects induced by four different test methods, (i.e. pull-off, slant shear, splitting prism and bi-surface shear test), and also examined the influence of the rough surface preparation. It follows that a comparative bond strength testing should involve the same experimental procedure and surface preparation.

Pull-off direct and indirect tests are widely used to characterize the bond behaviour because their simplicity. For instance, Bonaldo et al. (2005) [6] carried out an experimental investigation about bond strength between concrete substrate and repairing steel fibre reinforced concrete (SFRC) via pull-off tests. They found that an increasing in the strength of the overlay does not lead to an increase in the pull-off strength, which is significantly affected by the strength of the substrate.

As known, geometric discontinuities produce stress concentration and strain localization that can drive the delamination process, which generally starts in the neighborhood of the discontinuities of the overlay, particularly at its edges (Granju et al., 2004 [12]). However, the delamination phenomenon is strongly affected by cracks occurring both at the interface and within the substrate bulk (Courard et al., 2014, [8]).

Delamination formation and growth can be detected by different techniques. Among these, there are non-destructive methods (visual check, infrared thermography, chain drag, electromagnetic and acoustic methods), semi-destructive methods (coring, pull-off test), and a variety of experimental tests based on the monitoring of the displacement field at the interface between the substrate and the overlay by means of transducers (e.g. LVDT) or extensometers. Delamination can be induced either by external loads or by coactive stresses. In the first case, the delamination process is driven by the achievement of the ultimate tensile strength at the overlay as the external load increases; whereas in the second case, delamination is induced by a misfit strain between the substrate and the overlay (e.g. during thermal variation acting on the system) and it is driven by peeling stress which produces crack formation and growth in the overlay. A variety of analytical and numerical studies devoted to model the delamination phenomenon can be

found in Literature. All these studies assume a specific behaviour of the interface, which plays a key role to properly describe the formation and growth of crack delamination.

Delamination propagation can occur under mode I, II, III or mixed-mode loading conditions (Rikards et al., 1996, [24]). Recently, various models have been proposed to account for the mode loading conditions and the interlocking between the crack surfaces in the overlay, which strongly affect the bond strength in laminated systems (Courard et al., 2014) [8]. In particular, some Authors (e.g. Walter et al. 2003 [32], Sabathier et al. 2003, [25]) proposed analytical models taking into account the interaction between the interlocking shear force at the interface and the tensile force acting in the overlay layer. Granju et al. (2004) [12] carried out FE simulations to assess the stress at the crack tip of a debonding propagation. The interlocking effect was reproduced by inserting proper elements joining the faces of the crack in order to inhibit the crack opening. The interlocking effect on the delamination propagation between a substrate and an overlay was also analyzed by Tran et al. (2006b) [28], which found that drying shrinkage strongly affects the debonding propagation, increasing the rate of cracking growth². Through the same method, the effect induced by cycling loads on the debonding phenomenon between a concrete substrate and a thin cement-based overlay has been considered (Tran et al., 2007 [29]). Moreover, the effect induced by the Young modulus of the overlay, the fibre reinforcement, the ultimate tensile strength of the overlay and the bond strength between the overlay and the substrate were taken into account by these Authors, founding that a low Young modulus and a high strength can lead to a significant improvement of the resistance to delamination (Tran et al., 2006a) [27].

The present study deals with an experimental investigation aimed to assess the mechanical performances of concrete elements stiffened by casting one or more layers of polymer-modified cementitious repair mortar on its upper surfaces. The concrete elements reproduce load-bearing concrete ceiling beams widely employed as flooring systems for residential buildings. The investigation is focused on the mechanical behaviour of such elements under bending loading, with the aim to understand the failure mechanism occurring in the samples. In particular, the experimental study allows assessing if the collapse mechanism is driven by interfacial delamination between the

²Concerning the effects induced by shrinkage, see also Decter et al., 1997 [10]

overlays or by cracks formation and propagation from the tensile region to the compressive zone of the samples.

The paper is organized as follows. A detailed description of the experimental program is reported in Section 2. A mechanical model is then applied to predict the mechanical behavior of the samples, as reported in Section 3. The main results provided by the modelling, with particular reference to the moment-curvature curve and the load-deflection response, are reported in Section 4. By using a commercial FE package, the main results provided by a numerical simulation are reported and discussed in Section 5. Finally, conclusions are drawn in Section 6.

2. Experimental investigation

In the last decades many kinds of repairing cementitious mortars have been developed and commercialized. Polymer modified mortars, fibre reinforced mortars, high-strength mortars, shrinkage-controlled mortars, rapid curing mortars are currently used in civil engineering. Naturally, the performances of the reinforced structure mainly depend on the kind of mortar used.

In the present investigation, three popular mortars, widely used as repair products, have been tested. The realized specimens consist of pre-stressed, load-bearing concrete ceiling beams widely used for realizing floors of residential buildings. The cross section of the specimens consists of a 5 mm thick prefabricated brick element which interior is filled by a concrete cast reinforced by two pre-stressed steel bars having a diameter equal to 5 mm. Thus, the shape of the cross section of the concrete core resembles a rectangle 12 cm width and 4 cm thick. The steel bars are symmetrically placed with respect to the centre of the cross section. The bars are prestressed, thus making the concrete cross section almost entirely compressed. Two overlays made of repairing mortar have been applied at the upper surface of such beams to strengthen the specimens. In particular, a first layer 6 cm thick of a repairing mortar is casted on ceiling beams and, after a curing period variable from 4 hours to 24 hours, a second layer 2 cm thick of the same kind of repairing mortar is casted on the first one. These thickness values are chosen to simulate the behaviour of a ceiling beam reinforced by casting one or two layers of repairing mortar on its intrados. Thirty-height specimens having length equals to 520 mm and width equals to 110 mm were realized. The thickness of the specimens equals 140 mm. A sketch of the

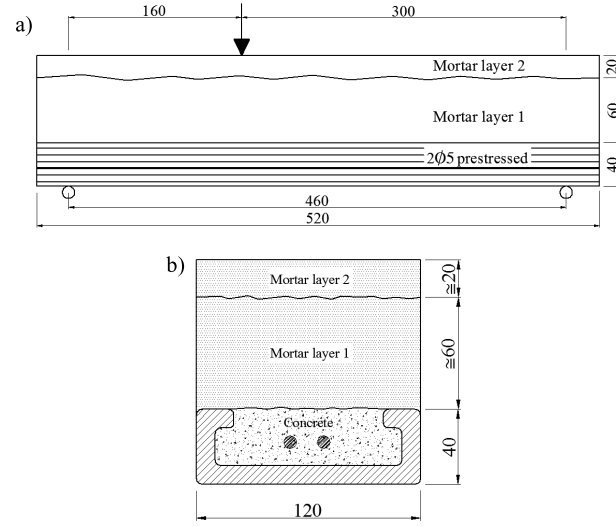


Figure 2: Sketch of the specimens under testing. Longitudinal view a) and cross section b).

beam-like specimens is reported in Fig. 2. Three different kinds of repair mortars have been used (see Section 2.1).

In order to assess the effect induced by curing, the layers of repairing mortar have been casted at different stages. In particular, before casting of the second layer, the first one has been cured for a period varying from 4 to 24 hours. The first overlay is 60 mm thick and the second is 20 mm thick. Both overlays have been casted manually. Before the casting of the second overlay, the surface of the first overlay has been wet and provided with a microtexture in order to promote adhesion. During the cast the temperature was equal to about 35 °C. The specimens differ each others by the kind of microtexture (obtained by using a metallic spatula or a brush, see Figure 3), the curing time of the first overlay during the cast of the second overlay (4, 12 or 24 hours) and intensity of surface wetting (light or intense). The abbreviations listed in Table 1 allow identifying the samples. In particular: "BLW" stands for brush and light wetting, "SLW" stands for spatula and light wetting, "SIW" stands for spatula and intense wetting, "S" stands for smooth light brushing finishing, "U" stands for a single overlay casted on the ceiling beam (instead of two mortar layers) and "NO B" stands for no B component (B component is an additive to promote the curing process of

Table 1: Denomination of specimens under testing

Denomination	
1) M1-12h-BLW	20) M3-12h-SLW
2) M1-NO B-SLW-A3	21) M3-12h-SLW
3) M1-24h-BLW	22) M2-24h-BLW
4) M1-24h-SLW	23) M2-4h-BLW
5) M2-4h	24) M1-NO B-24h S
6) M2-4h	25) M1-NO B-24h-BLW
7) M2-24h	26) M2-4h-BLW
8) M2-24h	27) M2-24h-BLW
9) M1-NO B-BLW-A1	28) M3-12h-SIW
10) M1-NO B-SLW-A4	29) M3-12h-SLW
11) M1-24h-S	30) M2-24h-BLW
12) M1-24h-SLW	31) M2-4h-BLW
13) M2-4h	32) M1-U-A2
14) M2-4h	33) M2-U
15) M2-24h	34) M3-U
16) M1-NO B-24h-S	35) M1-24h-BLW
17) M1-NO B-24h-BLW	36) M3-24h-S
18) M2-4h-BLW	37) M1-NO B-12h-S
19) M2-24h-BLW	38) M1-NO B-12h-S

the overlay increasing workability and compactness of the cast).

The main characteristics of the samples under testing are listed in Table 2. In this table wetting, kind of texture, the kind of mortar used to realize the overlay, curing time and presence of the adhesive activator between the concrete and the first overlay are reported in detail.

2.1. Materials used for realizing the samples

As reported above, specimens consist of pre-stressed, load-bearing brick ceiling beams with a core of reinforced concrete and stiffened with 1 or 2 overlays. Such layers are made of the same kind of repairing mortar. An adhesion activator has been applied to the free surface of the concrete core of some samples before casting the first overlay. Three different kinds of commercially available repairing mortar have been used and denoted with the following labels: M1, M2 and M3. M1 is a premixed, thixotropic, shrinkage

Table 2: Characterization of specimens

N. of samples	Label	Type of mortar	surface treatment of the 1 st layer	Curing time between 1 st and 2 nd layer	Activator of adhesion
1	1)	M1	brush	12h	/
1	2)	M1	spatula	12 h	A3
2	3), 11)	M1	smooth	24 h	/
2	4), 12)	M1	spatula	24 h	/
2	5), 13)	M2	no treatment	4 h	/
2	6), 14)	M2	no treatment	4 h	/
2	7), 15)	M2	no treatment	24 h	/
1	8)	M2	no treatment	24 h	/
1	9)	M1	brush	12 h	A1
1	10)	M1	spatula	12 h	A4
2	6), 14)	M2	no treatment	4 h	/
2	19), 27)	M2	brush	24 h	/
2	20), 28)	M3	spatula	12h	/
2	21), 29)	M3	spatula	12 h	/
2	22), 30)	M2	brush	24 h	/
2	23), 31)	M2	brush	4 h	/
1	32)	M1	Unique	/	A2
1	33), 33)bis	M2	Unique	/	/
1	35)	M1	brush	24 h	/
1	36)	M3	spatula	24 h	/
2	37), 38)	M1-No B	smooth	12 h	/

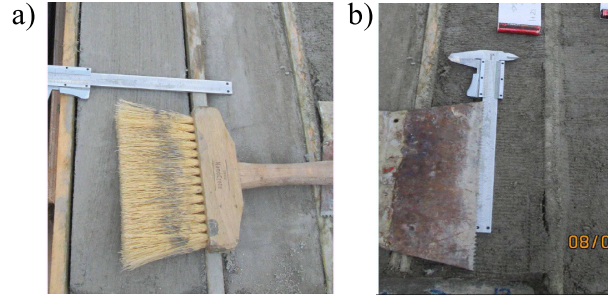


Figure 3: Tools used to impart a macrotexture to the surface of the first overlay. The brush a) and the metallic spatula b)

compensated cement mortar reinforced with Polyacrylonitrile (PAN) discrete fibres. M2 is a two-components, polymer-modified, cementitious mortar reinforced with PAN fibres containing an organic corrosion inhibitor. M3 is a fibre-reinforced, shrinkage compensated, repairing mortar. Four different kinds of adhesion activator have been used, here denoted by A1, A2, A3 and A4. A1 is an epoxy-based two-components fluid adhesion activator, slightly tixotropic, containing no solvents, that promotes adhesion among a wide class of building materials and guarantees good performances in terms of mechanical and chemical resistance. A2 is a mellow epoxy-based two-components adhesive activator, tixotropic and without solvents. A3 is a fluid vinyl-based adhesive promoter, compatible with each kind of solid support. A4 is a specific milky synthetic used to foster adhesion between cementitious elements. In order to prevent premature failure of the specimens near the edge supports, a bi-component styrene-free chemical anchor has been injected along the holes of the brick elements at the beam edges.

2.2. Ultrasonic testing

The samples have been subjected to ultrasonic tests. In particular, the travelling time of longitudinal as well as diagonal waves have been measured in order to identify cracks, voids and other discontinuities in the samples. Indeed, non destructive acoustic measurements (PND) are often used as a simple and efficient monitoring techniques to control damaging phenomena affecting the concrete elements. As known, acoustic measurement consists of evaluating the travelling time of ultrasonic wave pulses between an emitting transducer and a second receiving detector. An acoustic tester allows

assessing the transit time, rate, frequency and energy content of the wave pulses revealed by the receiving transducer, and, in turn, Young modulus, compressive strength and presence of defect can be inferred. In particular, presence of voids, cracks and inhomogeneities existing in a solid body can be identified because they produce a variation in the wave speed and a decrease of the amplitude of the wave.

The wave shape is visualized onto the display of a portable acoustic tester (see Figure 4). Ultrasonic testing have been carried out on the samples at different stages: during their realization, after curing, before and after the loading bending test, thus evaluating the residual strength of the concrete. The static Young modulus of concrete E_{static} can be related to the dynamic one $E_{dynamic}$ through the empiric Weber-Hermenn relation $E_{static} = E_{dynamic}/1.062$.

The compressive strength of the concrete has been determined by using the combined Son-Reb method [33] (recently, an alternative method based on the equivalency points has been proposed [30]). In particular, the impact rebound index (provided by sclerometric testing) has been related to the ultrasonic measurement to assess the characteristic compressive strength of concrete according to $R_{ck} = 1.2 \cdot 10^{-9} I_{rm}^{1.058} \cdot \nu^{2.446}$, being I_{rm} the (average) rebound index. The cylindrical compressive strength f_{ck} can be readily obtained from the cubic strength R_{ck} , being $f_{ck} = 0.83 \cdot R_{ck}$. The signals describing the wave propagation have been divided into 3 categories based on their regularity. Correspondingly, samples have been divided into 3 classes based on the shape of the signal revealed by the acoustic tester. In particular, label "REPETEABLE" stands for samples that exhibited acoustic signals having a regular shape in amplitude. This kind of curve denotes samples free of cracks and other failure phenomena. Label "FRACTURE" denotes samples that exhibited repeatable signals having an almost regular shape but characterized by small localized irregularities. "SLIT" stands for samples that exhibited not repeatable curves with a strongly irregular shape, thus denoting samples with cracks and significant material discontinuities. Figure 4 shows three kinds of revealed curves provided by ultrasonic testing. To assess the mechanical properties of the concrete, only the regular curves (i.e. the "REPETEABLE" signals) have been considered. The minimum values of the static Young modulus and the compressive strength of the concrete provided by SonReb method result $E_{static} = 33000$ MPa and $f_{ck} = 27.5$ MPa. Moreover, according to the technical information provided by the producer, the static Young modulus and cylindrical compressive strength of mortar M2

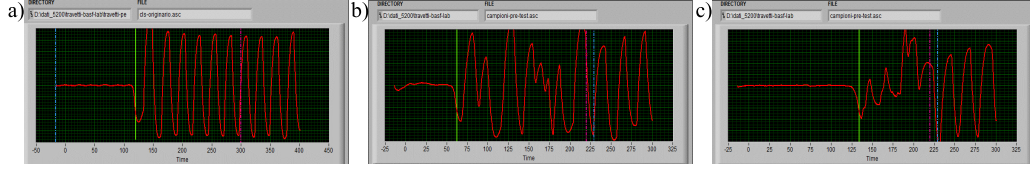


Figure 4: Curves provided by the ultrasonic testing equipment. Example of curve classified as "REPETEABLE" a). Example of curve classified as "FRACTURE" b). Example of curve classified as "SLIT" c).

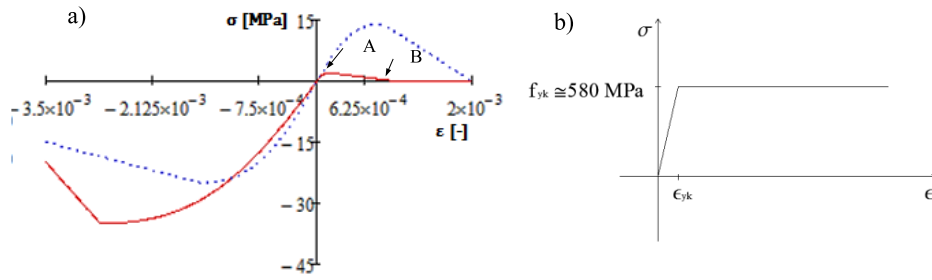


Figure 5: Constitutive laws for concrete (red line) and repair mortar M2 (blue dashed line) a), for the steel bars b).

have been taken equal to 25000 MPa and 45 MPa, respectively.

3. Modelling of the mechanical behaviour of the samples

To simulate the mechanical behaviour of the samples, the model of Arduini et al. (1997) [1] has been adopted. The contribution of the brick elements has been neglected, whereas the presence of a single or two overlays has been considered. According to the classical hypotheses for an Euler-Bernoulli beam and assuming perfect adhesion between concrete and steel reinforcement, the rotational equilibrium of the beam has been imposed. Therefore, by assuming nonlinear constitutive laws for concrete and steel, as reported in Figure 5, the theoretical moment-curvature curves have been obtained. In particular, as shown in Figure 5a, the behaviour of concrete adopted in the analysis is characterized by a softening branch starting from a strain of about $6.06 \cdot 10^{-5}$, whereas the stress-strain law for the repair mortar is linear until point "A", after that the stress monotonically decreases till point B, where

the strain equals $8 \cdot 10^{-4}$. At point B the stress is zero and, in turn, a crack is expected to take place.

For the steel bars, an elastic-perfectly plastic constitutive law has been adopted. In particular, the Young modulus is taken $2.1 \cdot 10^5$ MPa, and the characteristic ultimate and yielding stresses in tension are $f_{tk} = 1500$ MPa and $f_{yk} = 450$ MPa, respectively. It follows that the characteristic yielding stress can be found as follows (see Figure 5b):

$$f_{yk} = f_{tk} - \frac{N_{prestress}}{A_{steel}} = 580 MPa, \quad (1)$$

being $N_{prestress}/A_{steel} \cong 900$ MPa the pre-stress level in the steel bars. The procedure consists in varying the curvature of the cross section until the normal strain in the concrete beam at the extrados achieves the ultimate value prescribed by the standard regulation, i.e. 0.0035. Based on the constitutive law, the neutral axis and, in turn, the normal stresses taking place in the components (i.e. the concrete core, the steel bars and the overlays) are found, and the corresponding bending moment acting on the beam cross section is calculated. It is worth noting that also the concrete element is pre-compressed of about $900 \cdot 39.27/2800 \cong 12.62$ MPa, thus making the cross section entirely reacting before loading in bending. As the bending load increases, the state of pre-compression decreases, and the normal stress at the beam extrados becomes tensile. As known from the classical beam theory, the maximum value of the normal stress depends on the section modulus $W = bh^2/6 = 3.85 \cdot 10^{-3} m^3$. The moment-curvature curves for a bending loading provided by the theoretical model are reported in Figure 6. Each curve is related to a specific assumption: fully effective cross section, cross section without brick layers, fully effective cross section stiffened through a single overlay, cross section stiffened through a single overlay without brick layers and pre-stressed concrete cross section only. The maximum and ultimate values for the bending moments are listed in Table 3. By assuming a fully effective cross section (brown curve in Figure 6), the computation provides a maximum of the bending moment equals to 3.50 kNm; a bending moment at the end equals to 2.21 kNm and a stress level at the plateau of about 5.74 MPa. Correspondingly, the compressive stress at the lower fibre of the concrete core achieves 10.58 MPa and it corresponds to a point on the softening branch of the constitutive law of the concrete. The results show that perfect adhesion between the layers and absence of delamination can be stated if the maximum stress achieves the ratio of the maximum value of

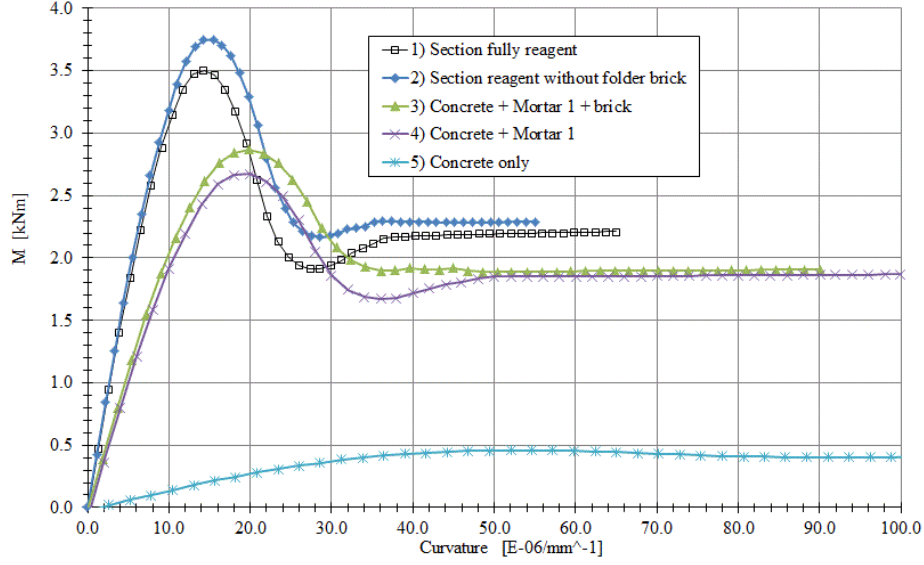


Figure 6: Moment-curvature relationship.

the bending moment 35000 Nm over the section modulus W , i.e. about 9.09 MPa, that represents the maximum stress level attainable. As the bending loading increases, the pre-existing stress level in the concrete decreases. The stress level attained in correspondence of the plateau of the moment-curvature curve allows to predict the failure mechanism. More specifically, if the stress corresponding to the plateau is greater (or equal) than 5.74 MPa, then delamination does not occur or it occurs in a localized region of the sample only. Conversely, if the stress corresponding to the plateau does not achieve this threshold, i.e. the stress remains minor than 5.74 MPa, it means that delamination occurs in the sample. Smaller the stress levels reached by the sample during flexure, greater will be the size of the region subjected to delamination. As displayed by Figure 6, it is found that despite the effect of the second overlay on the peak value of the bending moment be significant, it does not sensibly affect the stress level at the threshold. It follows that the delamination between the overlays is not meaningful. Conversely, the delamination between the concrete core and the first overlay significantly affects the mechanical response of the sample. Indeed, in this case, the bending moment at the plateau decreases from 1.86 kN till 0.43 kN. It can be inferred that, if the post peak stress level is very low, an extended delamination process has

Table 3: Peak and plateau values for the bending moment provided by the theoretical model and corresponding stress values

Cross section	Ultimate moment [kNm]	Peak moment [kNm]	Ultimate Stress [MPa]	Peak Stress [MPa]
1) Fully reagent	3.74	9.71	2.29	5.95
2) Fully reagent without folder brick	3.50	9.09	2.21	5.74
3) Concrete + Mortar 1 + brick	2.86	7.42	1.90	4.93
4) Concrete + Mortar 1	2.67	6.93	1.86	4.83
5) Concrete only	0.46	1.19	/	/

been took place.

As an example, from Figure 6 it is shown that the bending moment at the plateau of sample 1 is quite similar to that exhibited by sample 3. This fact means that a delamination process took place between the first and the second overlay in that sample. Owing to the fact that the thickness of the second overlay is small, the ultimate bending moment does not significantly differ from that of the sample 1. Conversely, sample 5 shown a ultimate bending moment at the plateau very small compared to the sample 2. This means that a delamination between the concrete and the first overlay occurred in that sample, and the loss of stiffness and the loss of the ultimate bending strength were very pronounced. It can be inferred that, if low values of ultimate post-peak bending moment is exhibited by a sample, in that sample a delamination process between the concrete and the first overlay takes place.

3.1. Three point loading bending test in a non-symmetric setup

A specific regulation to test the flexural behavior of stiffened ceiling beams for flooring does not exist. Therefore, in order to promotes delamination at the interface between the concrete and the first overlay and between the overlays of repair mortar and, at the same time, avoiding premature shear failure in the neighbourhoods of the edges of the sample, non-symmetric three-point loading bending test were performed (see Figure 2a). In particular, the length between the supports underlying the specimen was taken 420 mm, the load was applied on the specimen at 160 mm from the first support

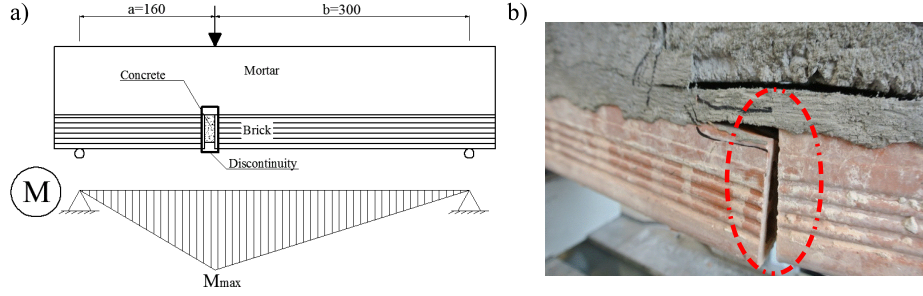


Figure 7: Sketch of the sample under non-symmetric three-point loading bending test a). Imagine of the collapse mode occurring in the sample during the bending test b).

and 300 mm from the other one, as reported in Figure 2. The bending tests have been carried out by controlling the deflection rate of the sample, equal to 0.2 mm/min.

4. Results

The samples have been realized with a material discontinuity in order to simulate the properties of the commercial ceiling beams. During the bending loading test, 23 of the 38 samples exhibited a mode I tensile crack propagates from the tensile zone of the sample in correspondence of the brick discontinuity. This is due to the fact that, in the neighborhood of the brick discontinuity, the concrete core is not bonded by the brick element, thus inducing there a stress and strain localization (see Figure 7). Thus, the brick discontinuity constitutes a preferential cross section for crack formation and growth. However, it seems that the peak tension achieved during the bending loading is almost uncorrelated to the position of the discontinuity in the brick element. Nonetheless, if the discontinuity lies near the maximum of the bending moment, a delamination process can take place there. Such phenomenon can be retrieved analyzing the experimental data concerning samples n. 6 and 14, realized with mortar M2. In the second one, the first crack started in the middle of the sample: the brick elements cracked and the crack propagates until the first overlay. In this sample the brick discontinuity is far to the maximum valued achieved by the bending moment. Conversely, in the sample n. 6 the first crack occurred in correspondence of the brick discontinuity, near the peak values of the bending moment. The

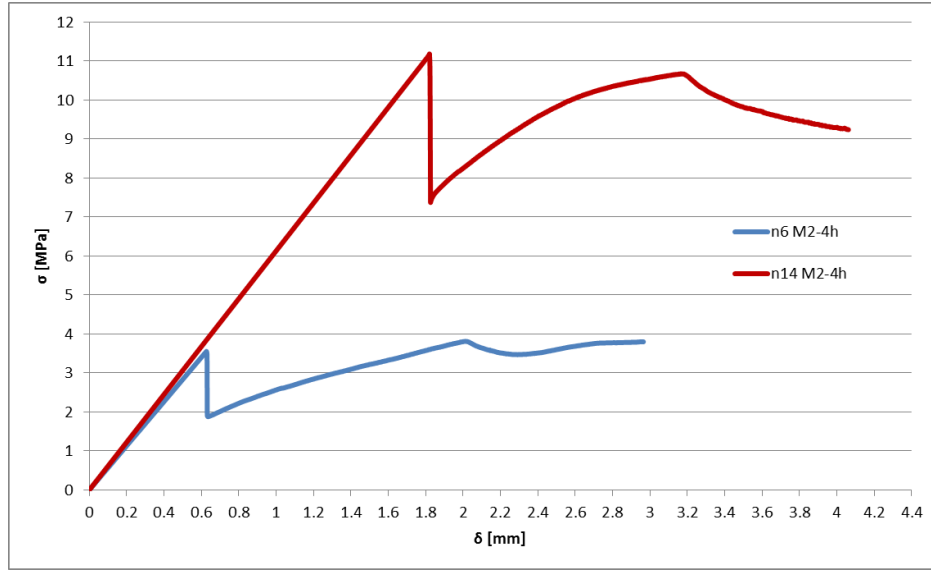


Figure 8: Experimental stress vs. deflection curve of samples n. 6 and 14.

response of such samples in terms of stress vs. deflection curve is shown in Figure 8. The curves are characterized by a different slope just after the first crack. In particular, the lower value of the slope exhibited by sample n. 6 is due to the fact that a slide takes place between the concrete core and the first overlay and/or between the two overlays in the region within the point of load application and the brick discontinuity. This fact produced a crack propagating almost horizontally in the sample.

Based on the data provided by the experimental investigation, it can be inferred that the adhesive activator gives a small increase in the first crack load, as depicted in Figure 9a, where the mechanical response of samples 1 and 9 are compared in terms of stress vs. transversal deflection. Both samples were realized with mortar M1, but in sample 10 an adhesive activator (A4) was used to promote adhesion between the concrete substrate and the first layer of repair mortar. An important aspect concerns the post cracking behaviour of the samples after reaching the peak load. In particular, a ductile behaviour is shown for samples 9 and 10, whereas samples 2 and 32 show a brittle behaviour. Indeed, sample n. 2 exhibited a rapid decrease of stress, particularly starting from a deflection of about 1.6 mm (see Figure 9b), thus making it the sample less performing among the samples under testing despite

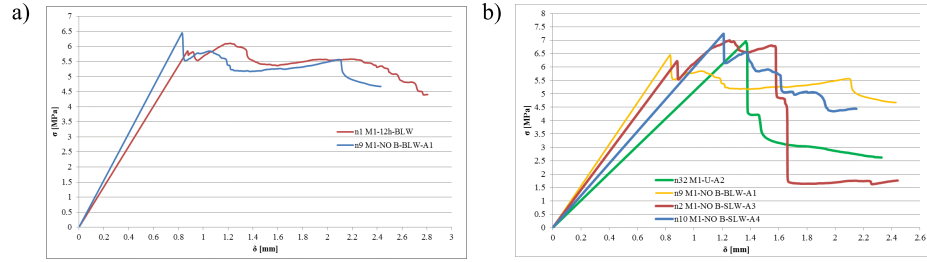


Figure 9: Experimental stress vs. deflection curve a) of samples n. 1 and 9; b) of samples 2, 9, 10, 32.

it exhibits high stress levels before cracking. Conversely, it can be stated that sample 9 is the most performing as it preserves a high stress level for a wide range of the transverse deflection after the occurrence of the first crack.

The first overlay of some samples (e.g. sample n.3) was realized by adding the B component to the mix. As showed by Figure 10, the B component seems to have a detrimental effect on the mechanical behaviour of the system. Indeed, the curve exhibited by sample 3 stays below the curve provided by sample 16, which has been realized without component B in the mix of the first overlay. Nevertheless, it is worth noticing that the samples realized without inserting the B component in the mix of the overlays are prone to a delamination process taking place between the overlays, whereas in samples realized by using component B the collapse occurs through a flexural crack propagating across the layers starting from the brick element. By considering the behaviour of samples n. 1, 3 and 4, that were realized with mortar M1 and B component, the effected induced by microtexture can be assessed. Note that the first overlay of sample 1 was provided with a microtexture realized with a brush, whereas in sample n. 4 the microtexture of the first overlay was realized with a metallic spatula; the first overlay of sample n. 3 was not provided with a microtexture. Figure 11 shows that sample 1 reveals a stiffness greater than the other samples, as it can be inferred by comparing the linear portion of the curves. Moreover, sample 1 exhibits a ductility greater than that displayed by the other samples. Indeed, the post cracking stress is higher than that shown by the other samples and almost constant for a relatively high values of the transverse deflection of the sample. It seems that both the curing period and the wetting of the surfaces of the first overlay do not sensibly affect the mechanical response of the samples.

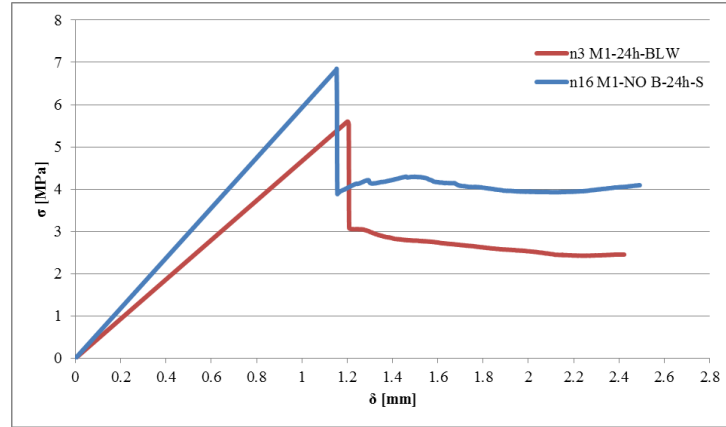


Figure 10: Experimental stress vs. deflection curve of samples n. 3 and 16.

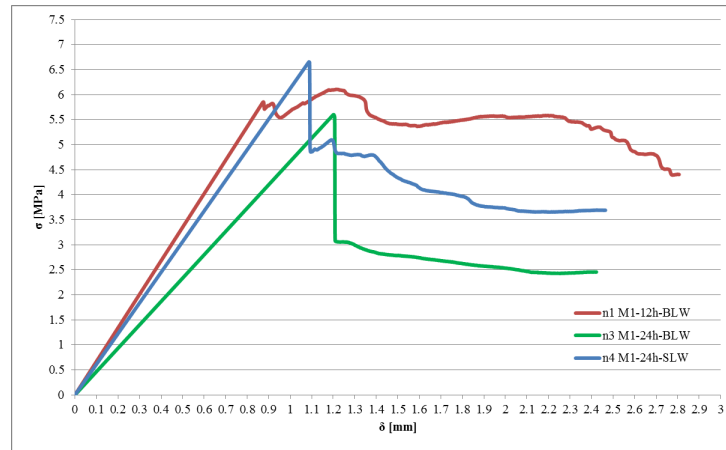


Figure 11: Experimental stress vs. deflection curve of samples n. 1, n. 3 and n. 4.

Table 4: Results provided by loading bending test on a group of specimens having the same characteristics.

N. of sample	Denomination	Kind of mortar	Surface treatment of 1 st layer	Curing time between cast of the 1 st and 2 nd layer
2	4, 12	M1	spatula	24 h
2	7, 15	M2	no treatment	24 h
2	16, 24	M1-No B component	smooth	24 h
2	17, 25	M1	brush	24 h
2	18, 26	M2	brush	4 h
2	20, 28	M3	brush	12 h
2	17, 25	M1	brush	24 h
2	18, 26	M2	brush	24 h
2	20, 28	M3	spatula	12 h
2	23, 31	M2	brush	4 h
2	37, 38	M1-No B component	smooth	12 h

It must be remarked that samples have exhibited different failure modes, so that a direct comparison among samples characterized by different wetting and curing conditions was not possible. The loading bending tests, carried out on samples having the same characteristics, allow identifying factors that can significantly affect the mechanical response of samples. The main results obtained by the bending tests are listed in Table 4.

Samples n. 16-24, 17-25, 18-26, 20-28, 23-31 revealed similar behaviour in terms of the maximum strength (the variation in strength does not overcome 1 MPa). Conversely, samples 4-12, 7-15 and 37-38 shown significant differences for both the peak value and the post cracking stresses. Such differences can be ascribed to the level of adhesion that takes place between the layers of the samples. In particular, the level of adhesion between the layers of samples 16 and 24 is similar as well as the flexural stiffness of these two samples (see Figure 12a). Conversely, the mechanical response of sample 37 significantly differs from that of sample 38. More specifically, sample

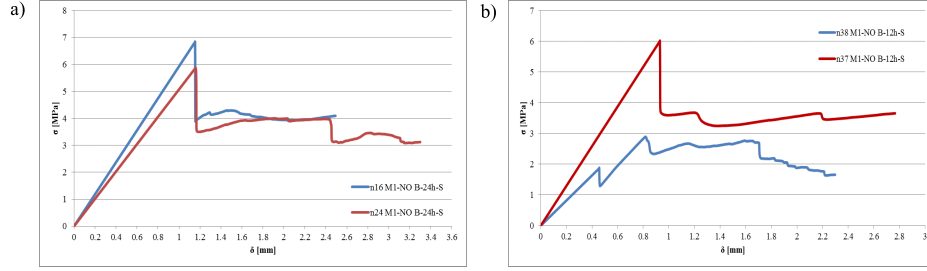


Figure 12: Results provided by loading bending test on samples a) 16 and 24 and b) 37 and 38.

38 exhibited a loss of stress due to a delamination occurred at the interface between the concrete substrate and the first overlay. On the other hand, the failure of sample 37 takes place without delamination, as shown in Figure 12b. This fact can be inferred by considering that delamination at the interface between the concrete of the ceiling beam and the first overlay or between the two mortar layers induces a significant loss of stiffness to the system. Indeed, after such a delamination took place, the layers detached from the underlying ones become inert and do not give significant supplies to the whole system in terms of flexural stiffness and bending strength. An almost horizontal post-peak behaviour of the load vs deflection curve can be ascribed to this phenomenon. Conversely, a local crack growth across the layers produce a sudden decrease of stress, after that an increment in the bending strength it is still possible due to the fact that the layers separated by the transverse crack maintain their resistance and, in turn, they bring stiffness and resistance to the sample.

Figure 13 shows the stress vs. deflection curves of samples that exhibited high values of strength. In particular, a comparison is made among samples 11, 12, 14, 15, 19 and 21 which have shown a peak stress higher than 9.09 MPa. Samples 11, 14 and 19 exhibited high strength levels. No delamination occurred in such samples in which, after a first localized crack, the stress can be increase until the collapse of the system without debonding processes between the overlays. This fact is confirmed by the hardening portion in the stress-deflection curve, as displayed by Figure 13. It is worth noticing that sample 21 shown a sudden decrease of the stress after an hardening branch. In fact a delamination process occurred in this sample until the complete debonding of the first overlay from the concrete beam. This gives to the

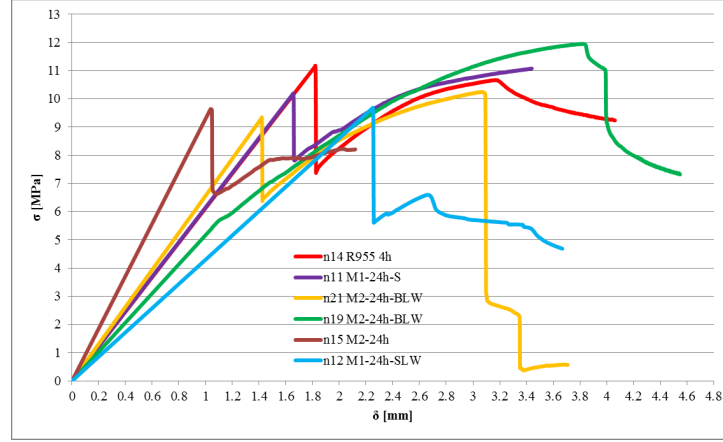


Figure 13: Results provided by loading bending test on samples exhibiting high performances.

sample 21 a brittle behaviour.

The comprehensive results provided by the experimental loading bending tests are reported in Figure 14. In particular, Figures 14a, 14c and 14e show the mechanical response of 3 classes of samples realized with mortar M2, M1 and M3 respectively, whereas Figures 14b, 14d and 14f display the corresponding envelopes in order to highlight the dispersion of the experimental data. The investigation encompasses 17 samples realized with mortar M2, 16 samples with mortar M1 and 6 samples with mortar M3. As shown, the experimental data are affected by an important spreading despite the fact that samples have been realized in the same environmental conditions and by using the same kind of mortar. In particular, an high fluctuation affects the peak of stress, the maximum value of the deflection and the stiffness at the beginning of the tests. This scenario is due to the following factors: the different kind of microtexture, the level of wetting, the curing time, the use or not of an adhesive activator and of the B component.

The comparison among the overall results is reported in Figure 15, where the envelopes of the stress vs. deflection curves are for each group of samples are shown. As it can see, the data concerning with samples realized with mortar M2 are affected by a less dispersion with respect the other classes of samples. Indeed, as shown by Figures 14a-b, the performances of samples realized with mortar M2 are less sensible to microtexture, the level of wet-

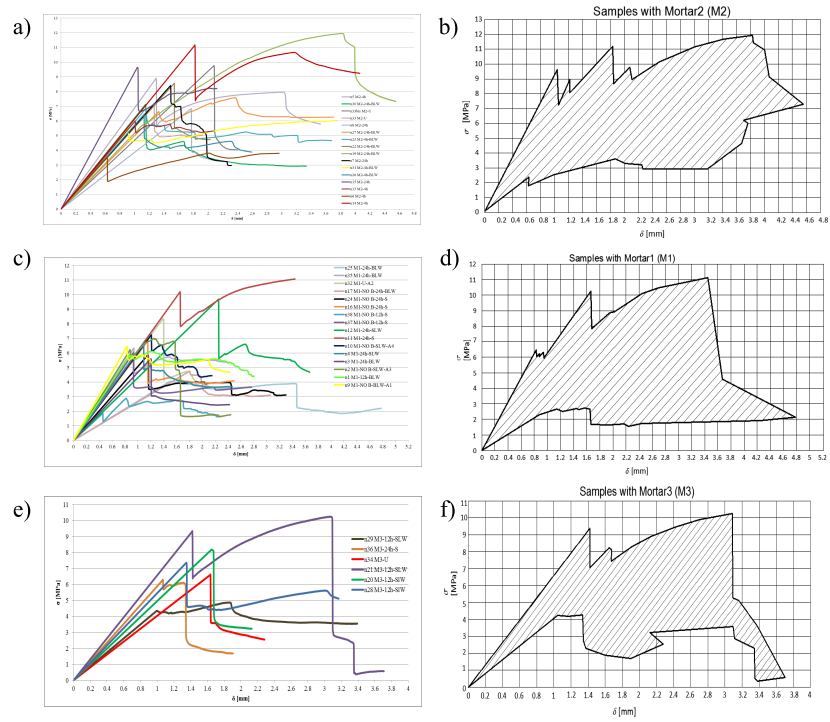


Figure 14: Results provided by loading bending test in terms of stress vs. deflection and corresponding envelopes. Samples realized with mortar M2 a)-b). Samples realized with mortar M1 c)-d). Samples realized with mortar M3 e)-f).

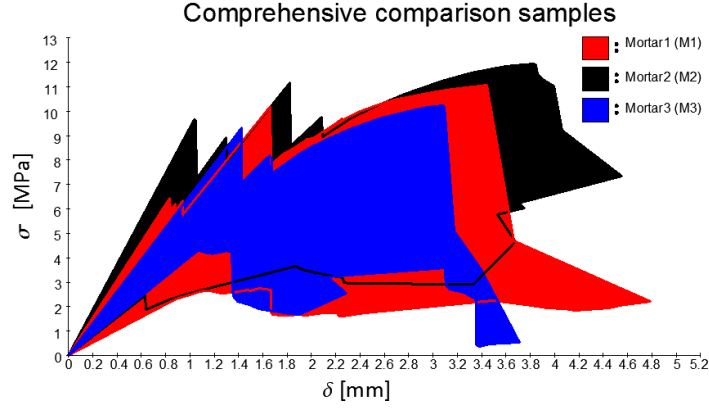


Figure 15: Comparison of the overall results provided by loading bending test.

ting and curing time. This makes such a class of samples more reliable and less sensible to these variables. Moreover, samples realized with mortar M2 exhibit a ductile behaviour; the stress-deflection curves are free of sudden loss of stress. Conversely, the remaining classes of samples (mortar M1 and M3) exhibit, in general, lower peak values of stress and a lower ductility with respect the first class of samples. Furthermore, a greater spreading affecting the experimental results can be recognized for these kinds of samples. By assuming a fully effective cross section of the sample, the theoretical simulation shows that 3 samples with mortar M2 overcome the stress of 9 MPa, whereas only 2 samples with mortar M1 and a single sample realized with mortar M3 achieved this stress level. Based on the experimental investigation, the samples realized with mortar M2 can be considered the most performing.

5. Numerical simulations

On the basis of experimental results, numerical FE models have been performed. For sake of simplicity, a linear elastic behaviour for the materials is assumed. The samples have been simulated by 2D plate elements. However, in order to reproduce the response of the samples revealed by the experimental investigation, an adaptive analysis has been performed by progressively diminishing the stiffness moduli of the materials as the load increases. The cracks have been simulated by assuming a vanishing elastic modulus for the plate elements lying where a crack developed during the loading bending test,

thus recovering step-by-step the load vs. deflection experimental curve.

Five kinds of plate elements have been used to simulate the concrete, the damaged concrete, the mortar layer staying below and above the neutral axis and damaged mortar. The brick element has been neglected because its contribution to the whole resistance of the system turns out to be meaningful. The reinforcing steel bars have been simulated by means of beam elements. The plate elements simulating the concrete are 70 mm thick, whereas those simulating the mortar overlays have a thickness equal to 110 mm. The numerical models simulate the three point loading bending tests, as sketched in Figure 16. The whole mesh includes 2600 plates having a size of 5 x 5 mm, 17 beam elements 520 mm long and 2730 nodes. Perfect adhesion has been considered between the layers, which have been assumed as homogeneous isotropic bodies.

Several numerical simulations have been carried out. In order to reproduce the experimental stress-deflection curves, the simulations have been developed through various steps. At first, a mesh reproducing the geometry of the samples has been performed, and appropriate values of the Young moduli of the layers have been adopted to retrieve the initial linear portion of the experimental curves. A second step consist of changing the 2D mesh by inserting elements having a vanishing Young modulus in the regions of the sample where a crack initiated and growth as noticed during the experimental tests.

In that follows, the results concerning the simulation of sample n. 15 M2-24h are reported owing to the fact that this sample exhibits a typical behaviour of a ceiling beam under three points loading bending test. The following mechanical parameters have been adopted to simulate the behavior of the sample through a FE model: for the concrete, from the SonReb method it has been obtained $E_{static} = 33000$ MPa, $f_{ck} = 27.5$ MPa. For mortar M2, the data provided by the producer are: $E_{M2,static} = 25000$ MPa, $f_{ck,M2} = 45$ MPa. For the steel bars, the mechanical parameters adopted in the numerical simulations are those reported in the previous Section. Before to realize the mesh, the position of the neutral axis need to be calculated; after that, the mesh can be carried out. Above the neutral axis, the elements are fully effective, whereas below it the plate elements are subjected to a tensile stress, thus for such plate elements a reduced Young modulus has been adopted. The value of the reduced Young modulus has been chosen in such a manner to reproduce the experimental stress vs. deflection curves through an iterative procedure. It is worth noting that the portion of the concrete below the

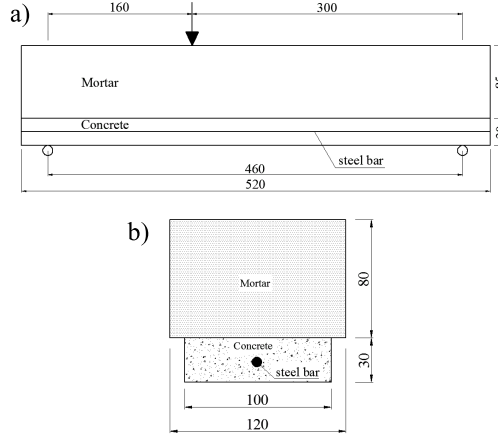


Figure 16: Sketch of the simulated sample under three-point loading bending test a) and its cross section b).

neutral axis has been considered fully effective due to the presence of pre-stress in such element. Nevertheless, taking into account that the reinforcing steel bars are not provided with a texture to improve adherence and that the pre-stress level in the concrete element is small, the pre-stress has not been accounted for in the numerical model. Based on the experimental curve, the non-symmetric loading bending test have been simulated, and the Young moduli of the plate elements have been chosen in order to retrieve step-by-step the experimental curve. In particular, for sample n. 15, the crack started in correspondence of the brick discontinuity at a load equal to 33208 N, then, the delamination process propagated between the concrete and the first overlay and, successively, the crack propagation occurred within the first overlay until the lower surface of the second overlay. After this, the crack propagated along the interface between the overlays and, finally, across the second overlay attaining the point load. Thus, delamination occurred at the interface of the concrete element and the first overlay as well as between this and the second one.

The procedure to carry out the numerical analysis can be subdivided in 4 steps. A first step is devoted to reproduce the initial linearly elastic portion of the stress vs deflection curve provided by the experimental investigation. To this aim, both the mortar above the neutral axis and the concrete are taken fully effective whereas the mortar staying below the neutral axis is

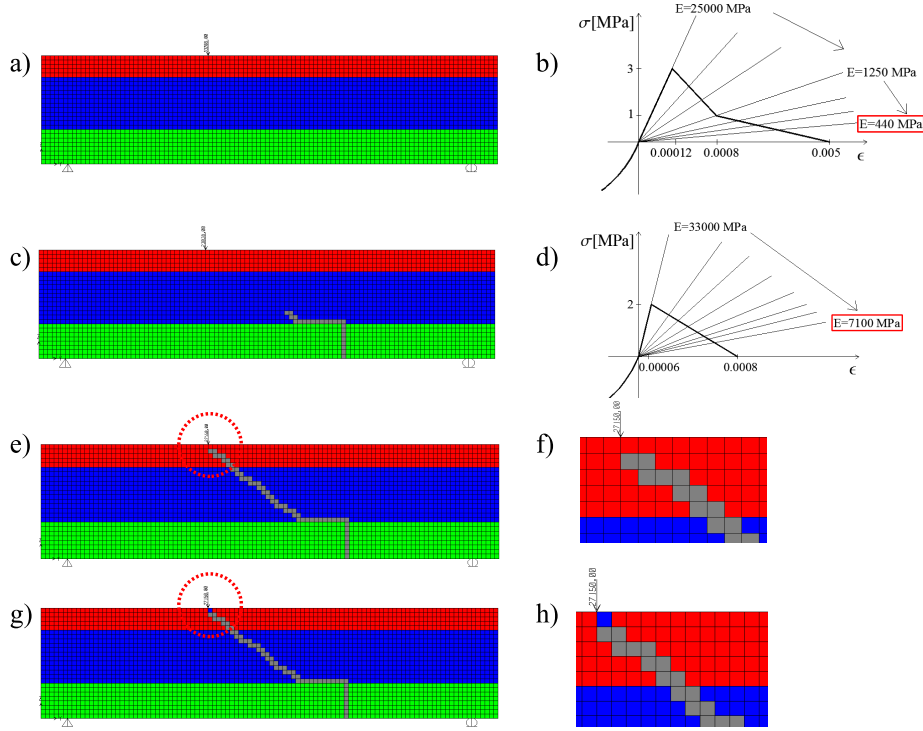


Figure 17: Step-by-step FE simulation to reproduce the mechanical behavior of sample n.15. Evolution of the FE mesh to reproduce the crack path experimentally observed a),c),e)-h). Reduction of the Young modulus of mortar M2 in order to reproduce the stress vs. deflection curve provided by the experimental investigation b),d).

partially effective, i.e. its Young modulus has been reduced to retrieve the initial portion of the experimental stress-deflection curve (see Figure 17a-b). The value of the external load adopted in the model was the same obtained by the experimental test until the end of the linear branch. In a second step, the end point of the softening branch of the experimental curve is identified. The corresponding value of the load is now adopted in the FE simulation and the 2D elements in the neighborhood of the position of the first crack are deleted. At this stage the position of the neutral axis remains the same of that calculated at the first step, moreover, since a damage process occurs in the concrete elements, a reduced Young modulus is attributed to the 2D elements simulating the concrete. Similarly, a reduced Young modulus equal to 440 MPa is adopted for the plate elements simulating the mortar layer

M2 below the neutral axis in order to reproduce the first linear portion of the experimental force vs. deflection curve. By means of an iterative procedure, the Young modulus for the concrete is progressively reducing until the stress-deflection curve provided by the FE analysis coincides with the softening branch of the experimental curve (see Figure 17c-d). The third step is intended to reproduce the hardening behaviour of the system after the end of the softening curve. To this aim, the load corresponding to the end point of this branch of the experimental curve is used in the FE model. At this stage, the simulation should reproduce the effect of the crack propagation across the first overlay. Thus, the plate elements near the position of the crack revealed by the experimental test are replaced with elements having a vanishing Young modulus (gray elements in Figure 17e). The crack propagates across the second overlay but it does not arrive at the end of it (see Figure 17f). Finally, in the last step the load corresponding to the end point of the post-cracking branch of the experimental curve is assumed in the FE model. The crack reaches the surface of the second overlay just under the point of load application (see Figure 17g-h). Also in this step, a progressive reduction of the Young modulus of the plate element near the point of load application is taken in order to reproduce the final portion of the experimental curve.

In the following, the load vs. deflection curve obtained by the numerical FE simulation is reported and compared with that provided by the experimental three-point bending tests. In particular, the results obtained by the linear FE analyses carried out by following the steps reported above are shown in Figure 18a. The four linear segments are reported in the picture varying the colors of the lines. By joining the end points of these linear segments, the whole load vs. deflection curve is retrieved. As shown by Figure 18b, the simulated curve agrees well with the experimental one.

6. Conclusions

The experimental investigation and the numerical simulations carried out shown that a suitable level of bond strength between the layers was obtained for all specimens. However, an high and constant level of interfacial adhesion is attained only if procedures are carefully followed and ambient conditions are constant. Moreover, significant variations of bond strength were observed among the specimens and this affected both the stiffness and the ductility of the samples as well as the behaviour of the samples just after the first crack.

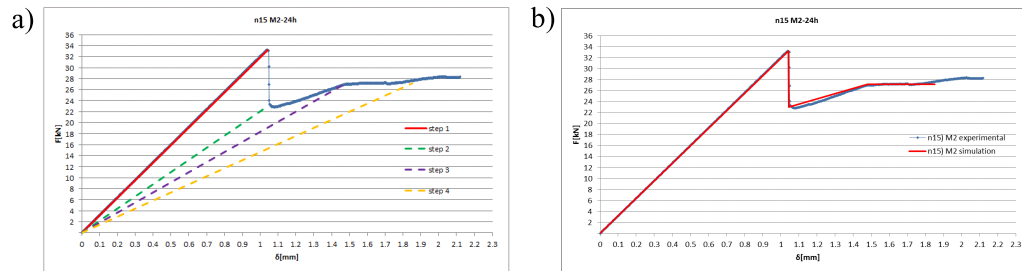


Figure 18: Load vs. deflection curve provided by the step-by-step FE simulation for sample n.15 a). Comparison between the experimental results and FE simulation in terms of load vs. deflection curve of sample n.15 b).

Although relatively simple, the performed FE model was able to predict the mechanical behaviour of stiffened concrete ceiling beams under bending loading. That numerical model is however not able to predict the crack formation and growth. So that the effect induced by cracks have been simulated by decreasing the Young modulus (until vanishing) for those plate elements positioned along the crack path in the specimens. This technique was also used for the plate elements lying in the neighboring of the interface and proved to be able to simulate the loss of adhesion, slip phenomena and other micro-damaging events affecting the behaviour of the interface.

References

- [1] Arduini M., Nanni A. Parametric Study of Beams with Externally Bonded FRP Reinforcement. *ACI Structural Journal* 1997, 94(5), 493-501.
- [2] Austin S., Robins P., Pan Y. Tensile bond testing of concrete repairs. *Materials and Structures* 1995, 28, 249-259.
- [3] Austin S., Robins P., Pan Y. Shear bond testing of concrete repairs. *Cement and Concrete Research* 1999, 29(7), 1067-1076;
- [4] Baluch, M.H., Rahman M.K., Al-Gadhib A.H., Risks of Cracking and Delamination in Patch Repair. *Journal of Materials in Civil Engineering ASCE* 2002, 14(4) 294-302;

- [5] Bissonnette B., Courard L., Fowler D.W., Granju J.-L. Bonded Cement-Based Material Overlays for the Repair, the Lining or the Strengthening of Slabs or Pavements State-of-the-Art Report of the RILEM Technical Committee 193-RLS, 2011, Springer
- [6] Bonaldo E., Barros J.A.O., Loureno P.B., Bond characterization between concrete substrate and repairing SFRC using pull-off testing. *International Journal of Adhesion and Adhesives* 2005, 25, 463-474;
- [7] Courard L., Garbacz A. Surfology, What does it mean for polymer concrete composites? *Restor Build Monum* 2010, 16(4-5):291-302
- [8] Courard L., Piotrowski T., Garbacz A., Near-to-surface properties affecting bond strength in concrete repair. *Cement and Concrete Composites* 2014, 46, 73-80
- [9] Di Leo A., Pascale G., Prove non distruttive sulle costruzioni in c.a. *Il giornale delle prove non distruttive* 1992, n. 4, (In Italian).
- [10] Decter M.H., Keeley C. Durable concrete repair: importance of compatibility and low shrinkage. *Constr. Build Mater.* 1997, 11(56), 267-273
- [11] Geissert D.G., Li S.E., Franz G.C., Stephens J.E. Splitting Prism Test Method to Evaluate Concrete-to-Concrete Bond Strength. *ACI Mater. J.* 1999, 96(3), 359-366
- [12] Granju J.-L., Sabathier V., Turatsinze A., Touni A. Interface Between an Old Concrete and a Bonded Overlay: Debonding Mechanism *Interface Science* 2004, 12, 381-388.
- [13] Júlio E.N.B.S., Branco F.A.B., Silva V.D. Concrete-to-concrete bond strength. Influence of the roughness of the substrate surface *Construction and Building Materials* 2004, 18, 675-681
- [14] Lanzoni L. Analysis of stress singularities in thin coatings bonded to a semi-infinite elastic substrate. *International Journal of Solids and Structures* 2011, 48(13), 1915-1926
- [15] Lanzoni L., Nobili A., Tarantino A.M. Performance evaluation of a polypropylene-based draw-wired fibre for concrete structures. *Construction and Building Materials* 2012, 28, 798-806

- [16] Lanzoni L., Tarantino A.M. Damaged hyperelastic membranes. *International Journal of Non-Linear Mechanics* 2014, 60, 922
- [17] Lanzoni L., Tarantino A.M. Equilibrium configurations and stability of a damaged body under uniaxial tractions. *ZAMP - Zeitschrift für angewandte Mathematik und Physik*, IN PRESS. doi: 10.1007/s00033-014-0397-6
- [18] Momayez A., Ehsani M.R., Ramezaniapour A.A., Rajaie H. Comparison of methods for evaluating bond strength between concrete substrate and repair materials. *Cement and Concrete Composites* 2005, 35(4), 748-757
- [19] Momayez A., Ehsani M.R., Ramezaniapour A.A., Rajaie H. Bisurface shear test for evaluating the bond between existing and new concrete. *ACI Mater. J.* 2004, 101(2), 99-106
- [20] Mehta P.K., Paulo Monteiro J.M. *Concrete: Microstructure, Properties, and Materials*. McGraw Hill Professional, 2013
- [21] Nobili A., Lanzoni L., Tarantino A.M. Experimental investigation and monitoring of a polypropylene-based fiber reinforced concrete road pavement. *Construction and Building Materials* 2013, 47, 888-895
- [22] Nobili A., Lanzoni L. On the stability loss for an Euler beam resting on a tensionless Pasternak foundation *ZAMP - Zeitschrift für angewandte Mathematik und Physik* 2014, 65(4), 797-808
- [23] Qian J., You C., Wang Q., Wang H., Jia X. A method for assessing bond performance of cement-based repair materials. *Construction and Building Materials* 2014, 68, 307-313
- [24] Rikards R., Buchhoiz F.-G., Bledzki A.K., Wacker G., Korjakin A. Mode I, mode II, and mixed-mode I/II interlaminar fracture toughness of GFRP influenced by fiber surface treatment *Mechanics of Composite Materials* 1996, 32(5), 439-462
- [25] Sabathier V., Granju J.-L., Bissonnette B., Turatsize A., Tamtsia B. Cement-based thin bonded overlays: numerical study of the influence of bond defects and fibre reinforcement *Proc. Int. Symp. „Brittle Matrix Composites 7* edite by A.M. Brandt, V.C. Li and I. H. Marshall,

eds. Warsaw, October 13-15, 2003 ZTUREK RSI and Woodhead Publ., Warsaw 2003

- [26] Tayeh B.A., Bakar B.H.A., Johari M.A.M., Voo Y.L. Evaluation of Bond Strength between Normal Concrete Substrate and Ultra High Performance Fiber Concrete as a Repair Material. *Procedia Engineering* 2013, 54, 554-563
- [27] Tran Q.T., Toumi A., Turatsinze A. Durability of an overlay-old concrete interface: the role of a metal fibre reinforcement. in *Brittle Matrix Composites 8*, 2006. Proceedings of an International Symposium, Warsaw, pp. 409-419
- [28] Tran Q.T., Toumi A., Granju J.-L. Experimental and numerical investigation of the debonding interface between an old concrete and an overlay. *Materials and Structures* 2006, 39, 379389
- [29] Tran Q.T., Toumi A., Turatsinze A. Modelling of debonding between old concrete and overlay: fatigue loading and delayed effects. *Materials and Structures* 2007, 40, 10451059
- [30] Viviani M., Glisic B., Scrivener K.L., Smith I.F.C., Equivalency Points: Predicting compressive strength evolution in three days, *Cement and Concrete Research* 2008, 38(8)-(9), 1070-1078.
- [31] Wall, J.S., Shrive, N.G. Factors Affecting Bond Between New and Old Concrete. *ACI Materials Journal* 1998, 85(2), 117-125.
- [32] Walter R., Stang H., Olesen J.F., Gimsing N.J. Debonding of FRC composite deck bridge in *Brittle Matrix Composites 7*, 2003. Proceedings of an International Symposium, Warsaw, October, Woodhead Publishing, pp.191200.
- [33] ASTM C597-02. Standard test method for pulse velocity through concrete, 2003.

List of Figures

1	Ceiling beams for flooring stiffened by a casted repairing mortar layer.	2
2	Sketch of the specimens under testing. Longitudinal view a) and cross section b).	7
3	Tools used to impart a macrotexture to the surface of the first overlay. The brush a) and the metallic spatula b)	10
4	Curves provided by the ultrasonic testing equipment. Example of curve classified as "REPETEABLE" a). Example of curve classified as "FRACTURE" b). Example of curve classified as "SLIT" c).	12
5	Constitutive laws for concrete (red line) and repair mortar M2 (blue dashed line) a), for the steel bars b).	12
6	Moment-curvature relationship.	14
7	Sketch of the sample under non-symmetric three-point loading bending test a). Imagine of the collapse mode occurring in the sample during the bending test b).	16
8	Experimental stress vs. deflection curve of samples n. 6 and 14.	17
9	Experimental stress vs. deflection curve a) of samples n. 1 and 9; b) of samples 2, 9, 10, 32.	18
10	Experimental stress vs. deflection curve of samples n. 3 and 16.	19
11	Experimental stress vs. deflection curve of samples n. 1, n. 3 and n. 4.	19
12	Results provided by loading bending test on samples a) 16 and 24 and b) 37 and 38.	21
13	Results provided by loading bending test on samples exhibiting high performances.	22
14	Results provided by loading bending test in terms of stress vs. deflection and corresponding envelopes. Samples realized with mortar M2 a)-b). Samples realized with mortar M1 c)-d). Samples realized with mortar M3 e)-f).	23
15	Comparison of the overall results provided by loading bending test.	24
16	Sketch of the simulated sample under three-point loading bending test a) and its cross section b).	26

17	Step-by-step FE simulation to reproduce the mechanical behavior of sample n.15. Evolution of the FE mesh to reproduce the crack path experimentally observed a),c),e)-h). Reduction of the Young modulus of mortar M2 in order to reproduce the stress vs. deflection curve provided by the experimental investigation b),d).	27
18	Load vs. deflection curve provided by the step-by-step FE simulation for sample n.15 a). Comparison between the experimental results and FE simulation in terms of load vs. deflection curve of sample n.15 b).	29